Hindawi
Journal of Nanotechnology
Volume 2018, Article ID 9808697, 7 pages
https://doi.org/10.1155/2018/9808697

Research Article

Assessment of Ruthenium Dye N719 Adsorption Kinetics in Mesoporous TiO_2 Films of Dye-Sensitized Solar Cells via Nanoplasmonic Sensing

Fahd M. Rajab [1,2]

[1]*Chemical Engineering Department, College of Engineering, Najran University, Najran, Saudi Arabia*
[2]*Promising Centre for Sensors and Electronic Devices (PCSED), Advanced Materials and Nano-Research Centre, Najran University, P.O. Box: 1988, Najran 11001, Saudi Arabia*

Correspondence should be addressed to Fahd M. Rajab; fmrajab@nu.edu.sa

Received 14 March 2018; Accepted 3 September 2018; Published 18 October 2018

Academic Editor: Raul Arenal

A dye monolayer formation on a semiconductor surface is critical for efficient dye-sensitized solar cells. The role of dye is to absorb light and convert it to photoelectrons, which are injected into the semiconductor conduction band as device current. We measured dye N719 adsorption via optical techniques including indirect nanoplasmonic sensing. The adsorption rate constant of dye N719 in mimic TiO_2 photoelectrodes is determined as $k_a = 983\ M^{-1}\ s^{-1}$. Dye adsorption for ruthenium dyes N3, N749, and Z907, coated onto TiO_2 photoelectrodes of varying thicknesses ranging from 3 μm to 10 μm, was conducted and related to fabricated dye-sensitized solar cell efficiency. Analytical studies included scanning electron microscopy and ellipsometry, X-ray diffraction, and UV-Vis spectroscopy, as well as quantum efficiency and current-voltage device characterizations. The results show greatest enhancement of device performance for dye N719 in spite of multilayer formation, which often is underestimated when addressing the dynamic competing factors that reverse thick-film device performance.

1. Introduction

The photovoltaic research community has focused on optimization of the photovoltaic device structure and material properties to enhance the conversion efficiencies [1]. Among the intensively researched photovoltaic device structures, the dye-sensitized solar cell (DSSC) provided an electrochemical research platform for converting light to electricity at large scale [2, 3]. DCCS main parts include a bandgap semiconductor film, a monolayer of organic dye molecules absorbed onto the semiconductor film, and a liquid electrolyte, which interpenetrates the dye-coated nanoparticles [4]. Electrons are injected into the conduction band of the wide bandgap semiconductor film, due to excitation energy introduced by incident photons, and then transferred through the film towards a current collector where they reduce the triiodide of the electrolyte [5]. A monolayer and uniform dye coverage by the semiconductor film is critical to improve the light harvesting efficiency. Excess dye loading can lead to multilayer formation, which causes quenching of the photoexcited electrons and leads to a reduction of charge injection [6]. On the contrary, poor dye coverage leads to the low photoactive surface area and an increased concentration of electron trap sites. Ono et al. [7] have shown that the agglomeration of dye molecules on titania surfaces causes high charge transfer resistance. The electron diffusion length is limited by a dynamic competition between electron diffusion and lifetime [8]. A high electron diffusion coefficient and a low recombination rate constant are key requirements for fabricating highly efficient dye-sensitized solar cells [9].

A majority of the research work on DSSCs has focused on the conventional dye N719 [bis(tetrabutylammonium)-*cis*-di(thiocyanato)-N,NA-bis(4-carboxylato-4A-carboxylic acid-2,2A-bipyridine)ruthenium (II)]. Other ruthenium dyes such as N3[*cis*-bis(isothiocyanato)bis (2,2′-bipyridyl-4,4′-dicarboxylato)ruthenium(II)], N749

[(2,2′:6′,2″-terpyridine-4,4′,4″-tricarboxylate)ruthenium (II) tris(tetrabutylammonium) tris(isothiocyanate)], and Z907 [*cis*-bis(isothiocyanato) (2,2′-bipyridyl-4,4′-dicarboxylato) (4,4′-di-nonyl-2′-bipyridyl)ruthenium(II)] differ in light absorbance and anchoring capability to semiconductor surfaces with varying highest occupied molecular orbital (HOMO) and lowest unoccupied molecular orbital (LUMO) levels [10]. The impregnation of the dye on the titania films occurs by soaking the matrix in a dye solution for several minutes to hours [11, 12]. The dye is adsorbed to the surface of titania by carboxylate groups that bind in different anchoring modes [13]. In order to fully characterize device performance with respect to dye coverage, it is essential to probe dye concentration throughout the entire film surface. Ellis-Gibbings et al. [14] used depth profiling to determine dye N719 multilayer formation on dye-sensitized solar cell photoelectrodes. Although a nondestructive absorbance technique can allow measurement of dye concentration for thin films, indirect nanoplasmonic sensing enables detecting diffusion at the lower interface of TiO_2 photoelectrodes by using nanoplasmonic gold sensors [15, 16].

In this paper, we probe dye N719 diffusion and adsorption kinetics via optical techniques including indirect nanoplasmonic sensing (INPS). Furthermore, we fabricate dye-sensitized solar cells using photoelectrodes of various thicknesses and impregnate them with ruthenium dyes N3, N749, and Z907 as well as with dye N719. We assess multilayer formation of dye N719 based on its adsorption kinetics and performance of fabricated devices in comparison with other dyes.

2. Experimental

2.1. Materials. Solutions containing ~3 wt% nanocrystalline titanium dioxide (Ti-nanoxide T(L)/SC), a paste containing ~18 wt% nanocrystalline titanium dioxide (Ti-nanoxide T/SP), ruthenium-based dyes N3, N719, Z907, and N749, Iodolyte AN-50, and Platisol were purchased from Solaronix. The particle size of the titanium dioxide is reported to be 13 nm. Precut fluorine-doped tin-oxide (FTO) films on glass substrates, serving as counter-electrodes, and commercial 60 μm thick spacers were also obtained from Solaronix. Acetonitrile and 2-methyl-2-propanol (*t*-butanol) were purchased from Fisher Scientific. Nanoplasmonic sensors of Au plasmonic nanodisks (diameter: 120 nm; height: 20 nm) with 10 nm dense layer of compact TiO_2 were obtained from Insplorion AB (Gothenburg, Sweden).

2.2. TiO_2 Photoelectrode Preparation. Titania films of various thicknesses were pasted using spin coating solutions Ti-nanoxide T(L)/SC for 700–775 nm mesoporous titania onto nanoplasmonic sensors (mimic photoelectrodes for nanoplasmonic analysis), 3–5 μm mesoporous titania on FTO glass utilizing a spin coater TOP8, and a screen-printing paste of Ti-nanoxide T/SP for 7–10 μm by the doctor blade method with the scotch tape (photoelectrodes for device fabrication). The thickness of the titania films was measured using Filmetrics F20 thin-film analyzer and VASE Ellipsometer VB-400 (Figure S1, Supporting Information). Anatase phase of titania is confirmed using XRD PANalytical X'Pert PRO (Figure S2, Supporting Information). Device films were fabricated with the same area of 0.384 cm^2. After the titania is applied, the mimic photoelectrodes were sintered on a hot plate at 100–500°C, while the device photoelectrodes were sintered at 500°C, all for 30 min.

2.3. Dye Impregnation and Device Fabrication. Solutions with a 3.0×10^{-4} M concentration of N3, N749, Z907, and N719 dyes are, respectively, prepared using 1 : 1 vol% acetonitrile/t-butanol mixture. The 3, 5, 7, and 10 μm films prepared are impregnated at times varying from 3 to 60 hours at a film temperature of 55°C, while the dye is kept at room temperature. Dye uptake is measured by taking sample readings of dye absorbance on solid titania films using UV-Vis Spectrometer Lambda 950 Perkin Elmer following a procedure described elsewhere [17]. Devices are constructed following a previous work by Rajab [18] using 60 μm spacers and characterized using a solar simulator IV-16 solar cell *I–V* measurement system from PV Measurements and QEX7 solar cell spectral response/quantum efficiency/IPCE measurement system from PV Measurements.

2.4. Nanoplasmonic Sensing of Dye Impregnation. Dye coverage is characterized by UV-Vis spectroscopy, and hence, uniform coverage is assessed for any particular film thickness. We fed 3.0 mM of N719 dye via a peristaltic pump of Insplorion XNano into mimic photoelectrodes to monitor the nanoplasmonic peak shifts (Figure 1). We were able to increase the effect of dye multilayer formation by using titania that can be sintered at a low temperature of 100°C revealing adsorption and desorption processes using a single dye loading in 60–90 minutes, (Figure S3(a), Supporting Information). We then use titania solution of typical sintering temperature at up to 500°C. The relatively slower adsorption kinetics of N719 dye on thicker films (faster saturation) is seen as lower slope of dye absorbance at 525 nm in Figure S3(b) (Supporting Information). We should mention that typical nanoplasmonic response of dye Z907 adsorption and desorption processes at TiO_2 photoelectrodes using Au nanosensors required Gusak et al. [19] to apply multiple dye loading and rinsing cycles.

3. Results and Discussion

Figures 2(b) and 2(c) show correlation of device quantum efficiency with ruthenium dyes absorption on 3 μm TiO_2 photoelectrodes. Devices with highest dye absorbance on solid titania films show highest short-circuit current and open-circuit voltage, corresponding with 3.72% of device efficiency (Figure 2(a) and see (a) in Table 1). Devices with dyes N749 and N3 and dye N719 show similar correlation of dye absorbance on TiO_2 photoelectrodes with short-

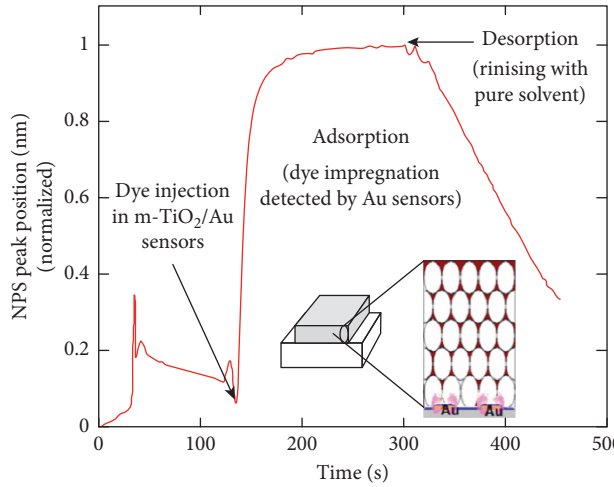

FIGURE 1: Nanoplasmonic response shows adsorption upon injection of dye into mesoporous titania on Au sensors followed by desorption upon rinsing with pure solvent.

circuit current, quantum efficiency, and device efficiency with 1.66% for dye N749, 1.10% for dye N3, and 0.95% for dye N719. This correlation is evident for device quantum efficiency and absorbance spectra of dyes N749 and N3 (Figures 2(b) and 2(c)), where both intersect at 585 nm. The open-circuit voltages for devices of dye N3 and dye N719 are 553 mV and 609 mV, respectively. Similar correlation of dye absorbance on TiO_2 photoelectrodes with short-circuit current and open-circuit voltage is seen for devices fabricated with 5 and 7 μm TiO_2 photoelectrodes, (Figures S4 and S5(a)–S5(c), Supporting Information).

For dye N719, the absorbance spectra on 10 μm TiO_2 photoelectrodes in Figure 3(b) are slightly higher than those of dye Z907 where their quantum efficiency spectra in Figure 3(c) are comparable. As mesoporous TiO_2 film thickness is increased, dye Z907 device efficiency improved by 24.2% due to 40.2% increase in short-circuit current with 2.9% drop in open-circuit voltage (see (b) in Table 1). Device quantum efficiency of dye Z907 dropped from 40% to 7% at 330 nm and from 50% to 8% at 520 nm (Figures 2(c) and 3(c)). However, dye N719 device efficiency improved 10 folds compared with dye Z907 due to increase in both short-circuit current and open-circuit voltage (see (a) and (b) in Table 1). Device quantum efficiency of dye N719 dropped from 42% to 6% at 330 nm but only from 11% to 8% at 520 nm (Figures 2(c) and 3(c)). The reduction of electron collection efficiency at (330 nm) is indifferent for both dyes Z907 and N719, whereas the reduction at 520 nm is more substantial for dye Z907, though their sensitization capability is similar of up to 750 nm. The proportional increase for dye N719 compared with dye Z907 with the increasing mesoporous surface area is a double effect of the low performance of dye N719 on 3 μm TiO_2 photoelectrode and of dye Z907 on 10 μm TiO_2 photoelectrodes. The latter is attributed to recombination effects resulting from multilayer formation of the bulky dye Z907 and comprised two hydrophobic groups. Gusak et al. used the INPS approach to determine the rate of adsorption of Z907 in similar porous titania films as 1384 M^{-1} s^{-1} [20].

For dye N719, however, recombination at longer wavelengths in both thin and thick TiO_2 photoelectrodes is likely due to multilayer formation hindering injection kinetics of low energy electrons. By inspection of the similar structure of dye N3, which lacks tetrabutyl ammonium salts, its 10 μm TiO_2 photoelectrode devices yield lowest quantum efficiency and device efficiency of 0.91% due to reduction in both short-circuit current and open-circuit voltage by 15.4 and 5.6%, respectively, in Figure 3(a)–3(c) and see in (b) Table 1. This shows that multilayer formation is likely indifferent for both dyes N3 and N719 on thick titania films. Gusak et al. [21] reported that dye N3 adsorption rate constant, k_a, ranges from 40 to 1000 M^{-1} s^{-1}. The partial enhancement of dye N719 is due to the additional two groups of tetrabutyl ammonium salt, which enhances its light absorption. In order to inspect the adsorption kinetics of dye N719, we used INPS to confirm the effect of sintering on multilayer formation and to determine the adsorption kinetics of dye N719.

Typical SEM images of Au sensor nanostructures and the as-coated mesoporous TiO_2 film are shown in Figures S3(c)–S3(d) (Supporting Information). As the mesoporous TiO_2 film is infiltrated with dye N719 solution, a resonance wavelength is used to reflect changes taking place at the surrounding environment of the bottom interface of the TiO_2 photoelectrode. This is referred to as nanoplasmonic peak shift, which plateaus upon saturation confirming dye diffusion to the lower TiO_2 interface.

Sintering of mesoporous films at high temperatures indeed minimizes film porosity and dye multilayer formation (Figure 4(a)), where the nanoplasmonic peak shifts of films sintered at varying temperatures show faster saturation for films sintered at higher temperatures. Dye N719 rate of adsorption is obtained by measuring the initial adsorption slope of N719 dye concentration (per film surface area), where the nanoplasmonic peak shift is inversely proportional to film thickness (Figure 4(b)). Dye N719 rate of adsorption, k_a, is determined as 983 M^{-1} s^{-1} (Figure 4(c)) confirming similar diffusion kinetics and multilayer formation to dye N3. For enhanced dye diffusion and electron

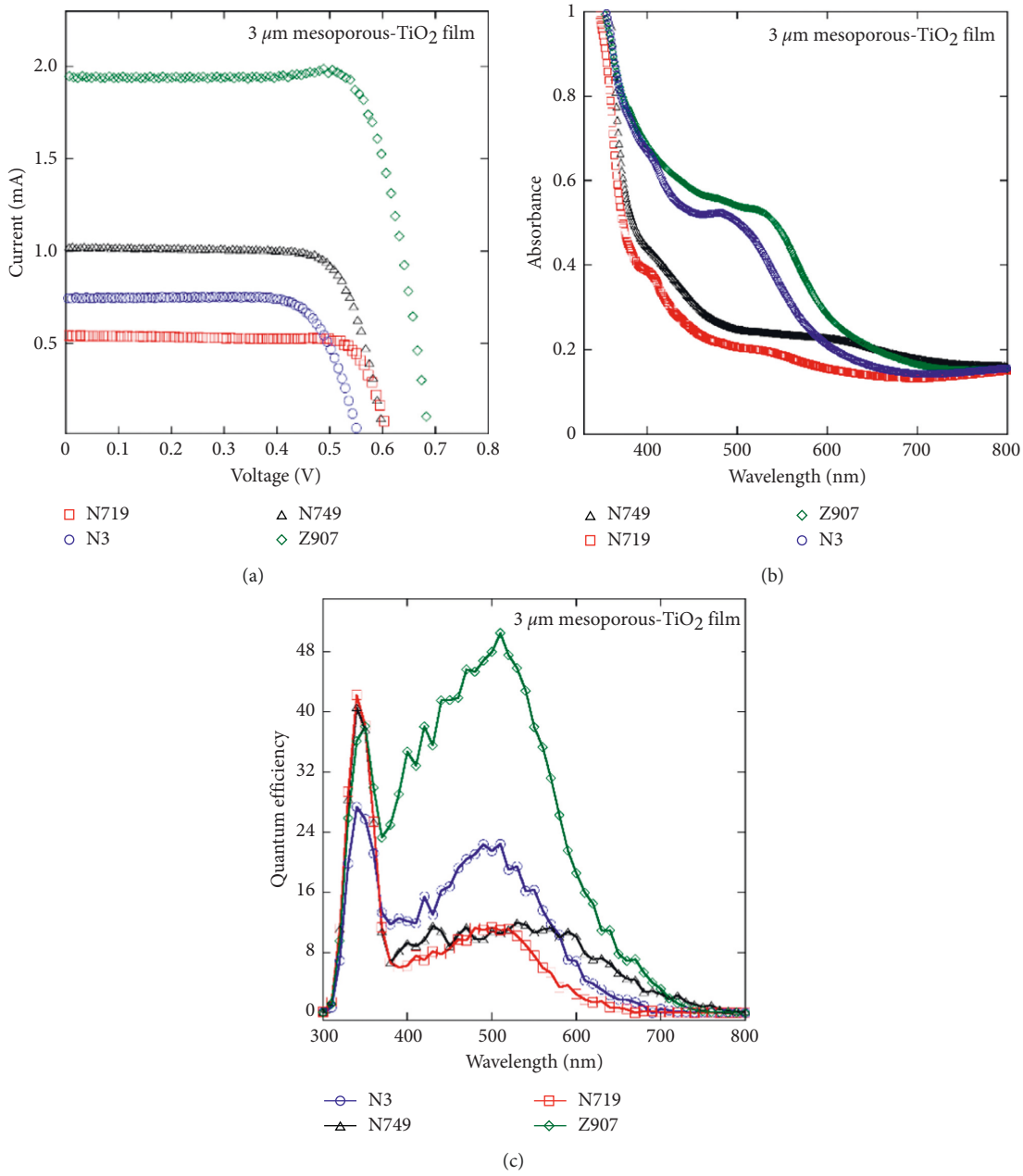

Figure 2: (a) IV and (c) quantum efficiency characteristic curves of devices fabricated with 3 μm mesoporous TiO_2 films using various ruthenium dyes N3, N749, Z907, and dye N719. (b) Absorbance at dye peaks on solid 3 μm mesoporous TiO_2 films show correlation with device quantum efficiency of respective dyes. Both device quantum efficiency in (b) and absorbance in (c) of dyes N3 and N749 show intersection at 585 nm.

collection efficiency, additional carboxylate groups of ruthenium dyes such as that of dye N749 in Figure 2(b) are likely to enhance dye adsorption kinetics, minimize multilayer formation, and optimize thick-TiO_2 photoelectrode device performance.

4. Conclusion

Ruthenium dye adsorption in mesoporous titania films is characterized using optical techniques by measurement of dye absorbance on TiO_2 photoelectrodes and indirect nanoplasmonic sensing. The kinetics of dye N719 adsorption via indirect nanoplasmonic sensing confirm multilayer formation similar to dye N3 that can be overlooked by the overall enhancement of electron collection efficiency of dye N719 devices. While multilayer formation is dominant for thick-TiO_2 photoelectrode devices, dye N719 device performance is improved due to its tetrabutyl ammonium groups. The dynamic data obtained via indirect nanoplasmonic sensing allow assessment of dye adsorption

Table 1: Short-circuit current density, open-circuit voltage, and efficiency of devices fabricated with (a) 3 μm and (b) 10 μm mesoporous TiO_2 films using dyes N3, N749, Z907, and N719.

	Isc (mA/cm^2)	Voc (V)	Efficiency (%)
(a) 3 μm			
N3	2.667	0.553	1.10
N749	3.642	0.602	1.66
Z907	6.940	0.687	3.72
N719	1.934	0.609	0.95
(b) 10 μm			
N3	2.250	0.523	0.91
N749	5.996	0.600	2.65
Z907	9.727	0.667	4.62
N719	6.833	0.672	3.25

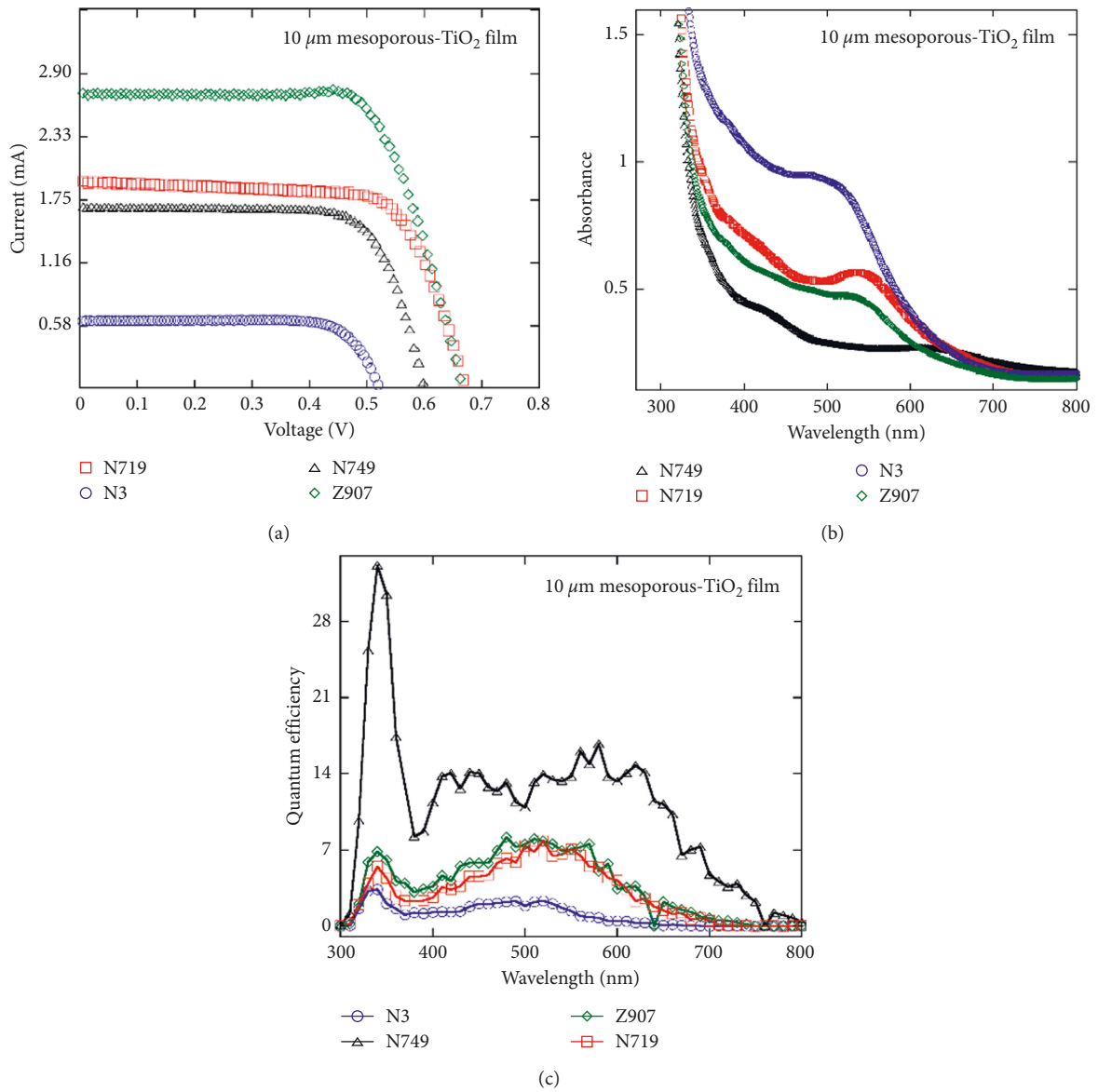

Figure 3: (a) IV and (b) quantum efficiency characteristic curves of devices fabricated with 10 μm mesoporous TiO_2 films using various ruthenium dyes N3, N749, Z907, and N719. (c) Absorbance of dyes on solid 10 μm mesoporous TiO_2 films shows inverse correlation with device quantum efficiency of respective dyes.

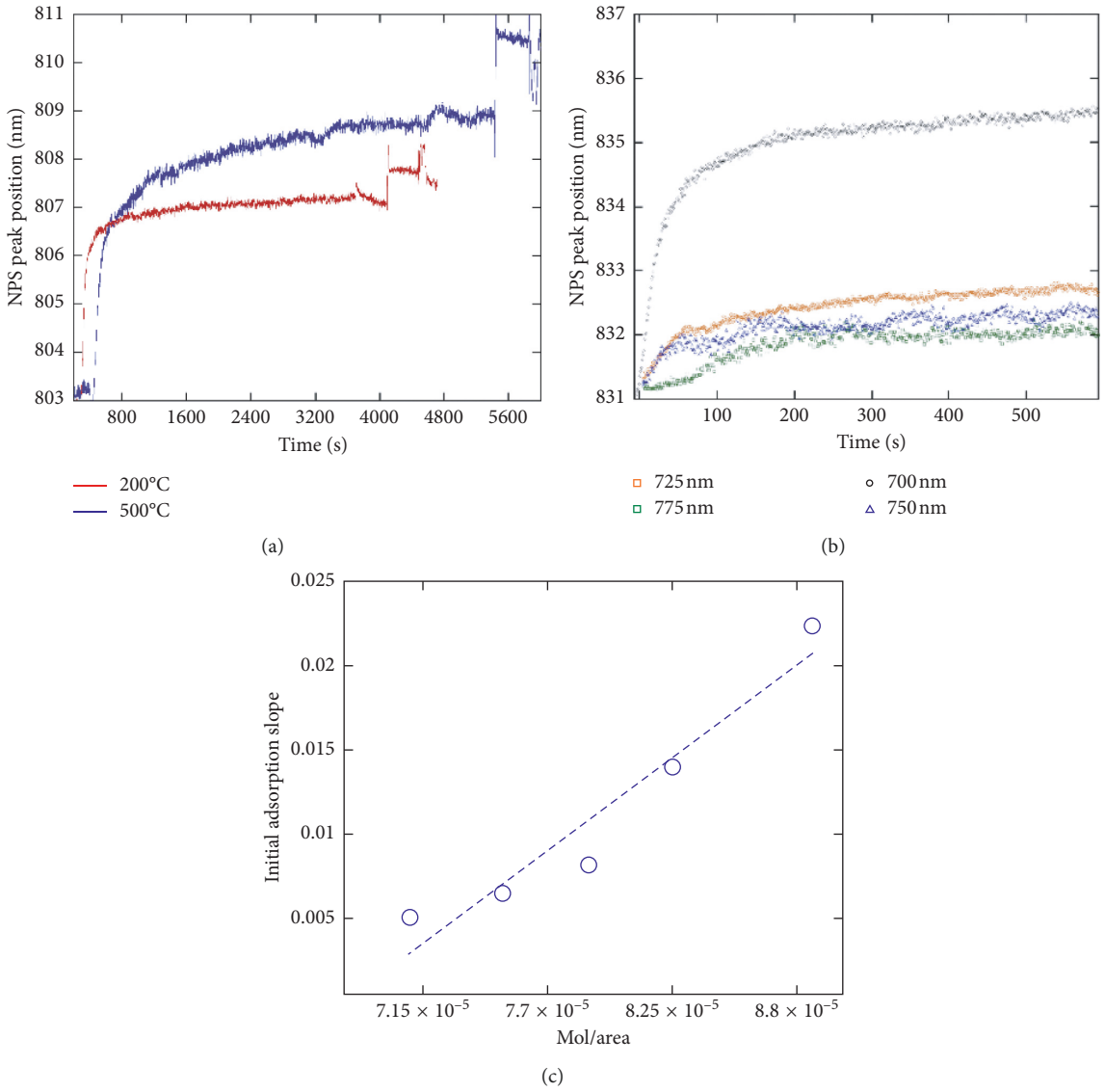

Figure 4: (a) Nanoplasmonic peak shifts upon injection of N719 dye into TiO_2 photoelectrode sintered at 200°C and 500°C. (b) Nanoplasmonic peak shifts of N719 dye in TiO_2 photoelectrodes of varying thicknesses from 700 nm to 775 nm. (c) Initial dye adsorption slope of the thinner films (700 nm film removed from data).

kinetics, providing an essential path towards specific dye, TiO_2 photoelectrode device optimization.

Data Availability

The data used to support the findings of this study are available from the corresponding author upon request.

Conflicts of Interest

The authors declare that they have no conflicts of interest.

Acknowledgments

The authors would like to acknowledge the support of the Ministry of Higher Education, Kingdom of Saudi Arabia, for this research through a grant (PCSED-003-16) under the Promising Centre for Sensors and Electronic Devices (PCSED) at Najran University, Kingdom of Saudi Arabia.

Supplementary Materials

Figure S1: ellipsometery measurement of TiO_2 photoelectrodes thickness. Figure S2: X-ray diffraction measurement of screen-printing Ti-nanoxide T/SP and spin coating Ti-nanoxide T(L)/SP mesoporous titania films shows peaks of anatase titania. Figure S3: (a) nanoplasmonic peak shifts indicative of (A) adsorption and (D) desorption of N719 dye into 700 nm and 725 nm TiO_2 photoelectrodes sintered at 100°C. (b) Faster saturation of N719 dye on thicker films reflected by lower slope of dye absorbance at 525 nm. Typical SEM images of (c) Au nanosensors and (d) mesoporous

TiO_2 film. Figure S4: (a) IV and (b) quantum efficiency characteristic curves of devices fabricated with 5 μm mesoporous TiO_2 films using N719, Z907, and N749 ruthenium dyes. (c) Absorbance at N719 and N749 dye peaks on solid 5 μm mesoporous TiO_2 films shows correlation with device quantum efficiency. Figure S5: (a) IV and (b) quantum efficiency characteristic curves of devices fabricated with 7 μm mesoporous TiO_2 films using N719, Z907, and N749 ruthenium dyes. (c) Absorbance at N719 and N749 dye peaks on solid 7 μm mesoporous TiO_2 films shows correlation with device quantum efficiency. (*Supplementary Materials*)

References

[1] S. Mathew, A. Yella, P. Gao et al., "Dye-sensitized solar cells with 13% efficiency achieved through the molecular engineering of porphyrin sensitizers," *Nature Chemistry*, vol. 6, no. 3, pp. 242–247, 2014.

[2] A. Hagfeldt, G. Boschloo, L. Sun, L. Kloo, and H. Pettersson, "Dye-sensitized solar cells," *Chemical Reviews*, vol. 110, no. 11, pp. 6595–6663, 2010.

[3] M. Grätzel, "Dye-sensitized solar cells," *Journal of Photochemistry and Photobiology C: Photochemistry Reviews*, vol. 4, no. 2, pp. 145–153, 2003.

[4] M. Adachi, M. Sakamoto, J. Jiu, Y. Ogata, and S. Isoda, "Determination of parameters of electron transport in dye-sensitized solar cells using electrochemical impedance spectroscopy," *Journal of Physical Chemistry B*, vol. 110, no. 28, pp. 13872–13880, 2006.

[5] A. C. Fisher, L. M. Peter, E. A. Ponomarev, A. B. Walker, and K. G. U. Wijayantha, "Intensity dependence of the back reaction and transport of electrons in dye-sensitized nanocrystalline TiO_2 solar cells," *The Journal of Physical Chemistry B*, vol. 104, no. 5, pp. 949–958, 2000.

[6] L. Zhang and J. M. Cole, "Dye aggregation in dye-sensitized solar cells," *Journal of Materials Chemistry A*, vol. 5, no. 37, pp. 19541–19559, 2017.

[7] T. Ono, T. Yamaguchi, and H. Arakawa, "Influence of dye adsorption solvent on the performance of a mesoporous TiO_2 dye-sensitized solar cell using infrared organic dye," *Journal of Solar Energy Engineering*, vol. 132, no. 2, article 021101, 2010.

[8] L. Peter, "Transport, trapping and interfacial transfer of electrons in dye-sensitized nanocrystalline solar cells," *Journal of Electroanalytical Chemistry*, vol. 599, no. 2, pp. 233–240, 2007.

[9] M. Sajedi Alvar, M. Javadi, Y. Abdi, and E. Arzi, "Enhancing the electron lifetime and diffusion coefficient in dye-sensitized solar cells by patterning the layer of TiO_2 nanoparticles," *Journal of Applied Physics*, vol. 119, no. 11, article 114302, 2016.

[10] N. Robertson, "Optimizing dyes for dye-sensitized solar cells," *Angewandte Chemie International Edition*, vol. 45, no. 15, pp. 2338–2345, 2006.

[11] D. Chen, F. Huang, Y. B. Cheng, and R. A. Caruso, "Mesoporous anatase TiO_2 beads with high surface areas and controllable pore sizes: a superior candidate for high-performance dye-sensitized solar cells," *Advanced Materials*, vol. 21, no. 21, pp. 2206–2210, 2009.

[12] Y. Jo, C. L. Jung, J. Lim et al., "A novel dye coating method for N719 dye-sensitized solar cells," *Electrochimica Acta*, vol. 66, pp. 121–125, 2012.

[13] L. Zhang and J. M. Cole, "Anchoring groups for dye-sensitized solar cells," *ACS Applied Materials & Interfaces*, vol. 7, no. 6, pp. 3427–3455, 2015.

[14] L. Ellis-Gibbings, V. Johansson, R. B. Walsh, L. Kloo, J. S. Quinton, and G. G. Andersson, "formation of N719 dye multilayers on dye sensitized solar cell photoelectrode surfaces investigated by direct determination of element concentration depth profiles," *Langmuir*, vol. 28, no. 25, pp. 9431–9439, 2012.

[15] C. Langhammer, E. M. Larsson, B. Kasemo, and I. Zorić, "Indirect nanoplasmonic sensing: ultrasensitive experimental platform for nanomaterials science and optical nanocalorimetry," *Nano Letters*, vol. 10, no. 9, pp. 3529–3538, 2010.

[16] E. M. Larsson, C. Langhammer, I. Zorić, and B. Kasemo, "Nanoplasmonic probes of catalytic reactions," *Science*, vol. 326, no. 5956, pp. 1091–1094, 2009.

[17] F. M. Rajab, "Novel nondestructive measurement of dye adsorption on solid Titania films for its sensitized solar cells," *Journal of Minerals and Materials Characterization and Engineering*, vol. 2, no. 3, pp. 169–175, 2014.

[18] F. M. Rajab, "Effect of solvent, dye-loading time, and dye choice on the performance of dye-sensitized solar cells," *Journal of Nanomaterials*, vol. 2016, Article ID 3703167, 8 pages, 2016.

[19] V. Gusak, L.-P. Heiniger, M. Graetzel, C. Langhammer, and B. Kasemo, "Time-resolved indirect nanoplasmonic sensing spectroscopy of dye molecule interactions with dense and mesoporous TiO_2 films," *Nano Letters*, vol. 12, no. 5, pp. 2397–2403, 2012.

[20] V. Gusak, L. P. Heiniger, V. P. Zhdanov, M. Gratzel, B. Kasemo, and C. Langhammer, "Diffusion and adsorption of dye molecules in mesoporous TiO_2 photoelectrodes studied by indirect nanoplasmonic sensing," *Energy & Environmental Science*, vol. 6, no. 5, pp. 3627–3636, 2013.

[21] V. Gusak, E. Nkurunziza, C. Langhammer, and B. Kasemo, "Real-time adsorption and desorption kinetics of dye Z907 on a flat mimic of dye-sensitized solar cell TiO_2 photoelectrodes," *Journal of Physical Chemistry C*, vol. 118, no. 30, pp. 17116–17122, 2014.